molecular pharmaceutics

pubs.acs.org/molecularpharmaceutics

Article

# Prediction of the Synergistic Glass Transition Temperature of Coamorphous Molecular Glasses Using Activity Coefficient Models

Xiao Zhao, Sixue Cheng, Yung P. Koh, Brandon D. Kelly, Gregory B. McKenna, and Sindee L. Simon*

Cite This: https://doi.org/10.1021/acs.molpharmaceut.1c00353

Read Online

ACCESS | Metrics & More | Article Recommendations

**ABSTRACT:** The glass transition temperature ($T_g$) of a binary miscible mixture of molecular glasses, termed a coamorphous glass, is often synergistically increased over that expected for an athermal mixture due to the strong interactions between the two components. This synergistic interaction is particularly important for the formulation of coamorphous pharmaceuticals since the molecular interactions and resulting $T_g$ strongly impact stability against crystallization, dissolution kinetics, and bioavailability. Current models that describe the composition dependence of $T_g$ for binary systems, including the Gordon−Taylor, Fox, Kwei, and Braun−Kovacs equations, fail to describe the behavior of coamorphous pharmaceuticals using parameters consistent with experimental $\Delta C_P$ and $\Delta\alpha$. Here, we develop a robust thermodynamic approach extending the Couchman and Karasz method through the use of activity coefficient models, including the two-parameter Margules, non-random-two-liquid (NRTL), and three-suffix Redlich−Kister models. We find that the models, using experimental values of $\Delta C_P$ and fitting parameters related to the binary interactions, successfully describe observed synergistic elevations and inflections in the $T_g$ versus composition response of coamorphous pharmaceuticals. Moreover, the predictions from the NRTL model are improved when the association-NRTL version of that model is used. Results are reported and discussed for four different coamorphous systems: indomethacin−glibenclamide, indomethacin−arginine, acetaminophen−indomethacin, and fenretinide−cholic acid.

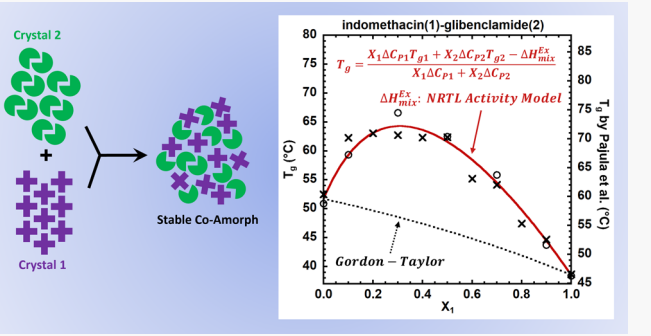


**KEYWORDS:** *stable coamorphous pharmaceuticals, glass transition temperature, activity coefficient model*



## INTRODUCTION

Amorphous or glassy materials can provide improved properties in numerous applications due to their lack of crystallinity and grain boundaries, including in the areas of pharmaceutical and energetic materials.[1−21] For example, in pharmaceuticals, amorphous drugs provide higher bioavailability and improved dissolution relative to their crystalline counterparts and, thus, lower doses relative to the toxic limit can be used,[1−19] whereas amorphous energetics are expected to show decreased shock sensitivity and improved performance relative to their crystalline counterparts.[20,21] The improved bioavailability and solubility of coamorphous solids may also find applications in agrichemicals and personal care and household products.[22] However, the downside of molecular (i.e., low-molecular-weight, nonpolymeric) amorphous solids is their tendency to crystallize during processing, storage, and use. One solution is the addition of polymeric binders or excipients, which are mixed with the low-molecular-weight glass former to form an amorphous solid dispersion, thereby increasing the glass transition temperature and reducing the potential for crystallization; however, the result is poor processability and often low loadings of the active components, leading to low energy densities for glassy energetic materials and, in the case of pharmaceuticals, requiring larger drug dosages and consequently reduced patient compliance. In addition, the hygroscopic polymers used as excipients in pharmaceuticals may result in the formulations being unstable in humid conditions. An alternative solution is the creation of stable coamorphous molecular glasses in which the interactions between two or more low-molecular-weight components are strong enough to prevent phase separation and crystallization of the pure components while, at the same time, ensuring that cocrystallization of the components is frustrated due to a mismatch of shapes or interactions between the components. Coamorphous pharmaceuticals are a relatively new develop-

Received: April 27, 2021
Revised: June 29, 2021
Accepted: June 30, 2021

ment in the drug delivery field and hold the promise of providing significant increases in drug dissolution rates, supersaturation levels, and bioavailability.[22−39]

The glass transition temperature, $T_g$, and the dynamics and kinetics of related phenomena, such as structural recovery and physical aging, are at the forefront of studies on coamorphous solids for a number of reasons. First and foremost, since crystallization during storage and use must be avoided, a brute force approach to making a stable coamorphous solid is to make $T_g$ as high as possible. By definition, molecular mobility is approximately the same for all compounds at their $T_g$ (with an $\alpha$-relaxation time of ∼100 s), and then, with decreasing temperature, mobility decreases roughly 1 decade every 20 K in the glassy state;[40] thus, the higher that we can elevate $T_g$, the more likely that we can obtain a glass that is stable against crystallization during storage,[41,42] explaining, in part, why polymer excipients have been commonly used with amorphous drugs despite their drawbacks with respect to hygroscopicity and processing.[43−48]

Perhaps more importantly, and less well explored, the $T_g$ of a coamorphous solid is reflective of the interactions between the two components,[16,23,24,49] and one of the goals of the present work is to develop the framework to predict and understand the relationship between the $T_g$ changes in coamorphous systems and the molecular-level interactions. The focus of this paper is on modeling systems in which there is a synergistic increase in $T_g$ due to strong specific interactions between the two components because that is important for coamorphous pharmaceuticals, but we note that coamorphous systems can also show negative deviations as in several polymer blends,[50−53] as well.

Based on the earlier work in polymeric systems, in the case of no interactions, the $T_g$ of a miscible amorphous binary mixture is well described by the Gordon−Taylor[54,55] or Kelley−Bueche equation[56]

$$T_g = \frac{X_1 T_{g1} + X_2 k T_{g2}}{X_1 + X_2 k} \quad (1)$$

where $X_i$ and $T_{gi}$ are the mole fraction and $T_g$ of species $i$, respectively, and the parameter $k$ is equated to the ratio of the step change in $(dV/dT)_T = V\Delta\alpha$ at $T_g$ of the two components $(V_2\Delta\alpha_2/V_1\Delta\alpha_1)$ or the ratio of the step change in the heat capacity $(\Delta C_{P2}/\Delta C_{P1})$, depending on whether eq 1 is derived from free volume theory[57] or configurational entropy theory.[58] Notably, the mole fractions used in eq 1 are interchangeable with weight fractions, as commonly used in the literature,[31,50,59] with the units of $V\Delta\alpha$ or $\Delta C_P$ used to determine the $k$ value being per mole or per gram, depending on which is used. Couchman and Karasz[60,61] have also derived eq 1 by considering the nominal glass transition to be an Ehrenfest second-order transition with entropy (or enthalpy or volume) being continuous at $T_g$. A simplification of eq 1 involving the Simha−Boyer approximation that $\Delta\alpha T_g$ is constant[62] results in the widely used Fox equation[63]

$$\frac{1}{T_g} = \frac{w_1}{T_{g1}} + \frac{w_2}{T_{g2}} \quad (2)$$

where $w_i$ is the weight fraction of component $i$.

Importantly, eqs 1 and 2 predict that the $T_g$ of a mixture lies between the component $T_g$ values and varies monotonically, and smoothly, between them. However, in the case of strong interactions,[64] the possibility of nonmonotonic or synergistic behavior exists as is observed in a number of molecular systems, including carvedilol with benzoic, maleic, and citric acids,[25] and several drug/amino acid systems.[26,27,30,31,34,35,37] The effect of specific interactions was recognized by Kwei,[49] who modified the Kelley−Bueche equation (eq 1) to account for hydrogen bonding in polymeric mixtures

$$T_g = \frac{w_1 T_{g1} + w_2 k T_{g2}}{w_1 + w_2 k} + q w_1 w_2 \quad (3)$$

where the second term represents the influence of the number of hydrogen bonds or specific interactions in the system and where $q$ is an adjustable parameter. This formulation is similar to the second-order concentration term used in the Jenckel−Heusch[65] equation. Equation 3 is also similar to the Braun−Kovacs[66] equation that was developed based on the assumption of the additivity of the parameter $B$ in Doolittle's[67] viscosity equation at the glass transition, leading to an iso-free volume surface at $T_g$, with the excess volume also given by a term that is second-order in concentration $qX_1X_2$

$$T_g = \frac{X_1 T_{g1} + X_2 k T_{g2} + q X_1 X_2}{X_1 + X_2 k} \quad (4)$$

where $q$ again is an adjustable parameter. It is also again emphasized that in eq 3 or 4, either mole or weight fractions can be used with $k$ adjusted accordingly. Both the Kwei and Braun−Kovacs equations can predict nonmonotonic increases in $T_g$; however, the equations assume that the interactions are a maximum for either a 50/50 weight or mole fraction mixture, respectively. Then, without taking the parameter $k$ as a fitting parameter, they are unable to describe systems in which there is unusual synergy such that the $T_g$ change relative to the "ideal" case of the Gordon−Taylor or Fox equation is asymmetrical with respect to composition. Of course, a symmetrical model in terms of mole fraction will become asymmetrical in terms of weight or volume fraction, but even so, the point of maximum deviation from the ideal $T_g$ behavior given by the Gordon−Taylor or Fox equation is predetermined by the molecular-weight difference and the $k$ value; hence, it is found that $k$ needs to be taken as a fitting parameter to provide the Kwei and Braun−Kovacs equations with sufficient flexibility to fit highly asymmetric data.

From a theoretical perspective, the synergistic elevation of $T_g$ has also been considered in the Flory−Huggins framework, in addition to a configurational entropy framework. However, as shown by Kim et al.,[68] the model requires the knowledge of lattice coordination number and still uses the strength of the specific interactions as fitting parameters. On the other hand, the synergistic interactions were theoretically interpreted in the Painter−Coleman association model,[64] where Couchman and Karasz's[60] approach was extended by counting the self- and cross-association interactions in the liquid state; the model successfully predicts the maximum $T_g$ for the coamorphous mixture of poly(vinyl pyridine) and poly(vinyl phenol) and requires no fitting parameters, although the association strength and population need to be predetermined by infrared spectroscopic measurements.

In this study, we aim to develop a framework to predict the synergistic $T_g$ behavior while maintaining the physical significance of the parameters. The intermolecular interactions, or nonideal mixing, are accounted for by activity coefficient models. Such activity coefficient models have been extensively used to describe and predict phase equilibria in nonideal


https://doi.org/10.1021/acs.molpharmaceut.1c00353
Mol. Pharmaceutics XXXX, XXX, XXX−XXX

systems, including but not limited to polymer solutions,[69−72] hydrogen-bonding fluids,[73−76] and ionic solutions.[77−80] Furthermore, activity coefficient models can be combined with perturbation theories to describe complex association interactions.[81,82] Here, we develop our model and then show predictions of $T_g$ as a function of the composition for multiple pharmaceutical coamorphous systems within a framework that uses activity coefficient models to describe the nonideal mixing. The results are compared to predictions using the Gordon−Taylor, Kwei, and Braun−Kovacs equations. The investigation includes analysis of $T_g$ data for four coamorphous systems: indomethacin−glibenclamide, indomethacin−arginine, acetaminophen−indomethacin, and fenretinide−cholic acid. The data come from calorimetric measurements of the glass transition temperature as a function of composition and are measured in this study and/or obtained from the literature.

## METHODOLOGY

**Derivation of the Model.** The model is derived as shown below for a binary mixture, and extrapolation to a multiple-component system is unchallenging and will not be shown. Based on the Painter−Coleman association model's[64] framework, we interpret the specific interactions in the liquid state by the excess enthalpy, $\Delta H^E_{liq}$, a well-defined thermodynamic property that represents the enthalpy difference between the real and ideal (athermal) mixtures

$$T_g = \frac{X_1 T_{g1} + X_2 k T_{g2} - \Delta H^E_{liq}/\Delta C_{P1}}{X_1 + X_2 k} \tag{5}$$

and

$$k = \frac{\Delta C_{P2}}{\Delta C_{P1}} \tag{6}$$

Notably, Painter et al. attributed the temperature dependence of $\Delta C_p$ to the self-association among species themselves, and this temperature-dependent association strength can be accounted for when assuming $\Delta H^E_{liq}$ is temperature-dependent in our method, such as for the association-non-random-two-liquid (NRTL) model that will be shown below.

The excess enthalpy is theoretically expressed in terms of mole fraction and the activity coefficient, $\gamma$, of species $i$ (=1 or 2)

$$\Delta H^E_{liq} = RT(X_1 \ln \gamma_1 + X_2 \ln \gamma_2) \tag{7}$$

where $R$ denotes the gas constant. The activity coefficient as a function of composition (or temperature) can be estimated, empirically or theoretically, by activity coefficient models,[83,84] of which the simplest one is the empirical one-parameter Margules model[85]

$$\Delta H^E_{liq} = RTA_{12} X_1 X_2 \tag{8}$$

Here, $A_{12}$ is a constant that indicates the strength of the specific interactions. Equation 8 results in a correction similar to the Braun−Kovacs equation (eq 4). The two-parameter Margules model[85] adds more complexity

$$\Delta H^E_{liq} = RTX_1 X_2 (A'_{21} X_1 + A'_{12} X_2) \tag{9}$$

where $A'_{12}$ and $A'_{21}$ are the adjustable parameters that describe a composition-dependent strength of the binary interactions. Moreover, expressions for the interactions that could be multibody, such as the three-suffix Redlich−Kister activity coefficient model,[86] may be useful to describe more complex binary or higher-order interactions

$$\Delta H^E_{liq} = RTX_1 X_2 [B_{12} + C_{12}(X_1 - X_2) + D_{12}(X_1 - X_2)^2] \tag{10}$$

where $B_{12}$, $C_{12}$, and $D_{12}$ are adjustable parameters. It is important to note that in all of these models, as well as the NRTL model discussed below, the model parameters are directly related to the strength of specific interactions, and these interactions are not a function of composition. However, the excess enthalpy, itself, is a function of composition because even for a binary mixture of A and B molecules, the probability of A−A, B−B, and A−B interactions changes with composition.

Further complexity, in comparison to the two-parameter Margules model, and with a theoretical connection to the underlying interactions, is obtained using the non-random-two-liquid theory (NRTL)[87] in which the intermolecular interactions result in differences between local and bulk concentrations, as originally suggested by Wilson's local composition theory[88]

$$\Delta H^E_{liq} = RTX_1 X_2 \left( \frac{\tau_{12} G_{12}}{X_1 G_{12} + X_2} + \frac{\tau_{21} G_{21}}{X_1 + X_2 G_{21}} \right) \tag{11}$$

and

$$G_{ij} = \exp(-\alpha_{ij} \tau_{ij}) \tag{12}$$

Here, the $\tau_{ij}$ are the normalized local interaction energies between the component $i$ around $j$ relative to those among the component $j$ themselves, which is assumed to be temperature-independent in the present study; $G_{ij}$ represents a weighting factor that accounts for the local composition relative to the overall composition; $\alpha_{ij}$ is a nonrandomness parameter that has been shown to be related to the reciprocal of the coordination number of the lattice, which is expected to be a positive constant of the order 0.1−0.3 for coordination numbers on the order of 6−12. In the present study, $\alpha_{ij}$ is taken to be 0.3 as is often suggested in the literature.[87,89,90]

Although the NRTL model often better describes non-idealities than does the two-parameter Margules model, it has been shown to insufficiently correlate association interactions[82,91] as it requires multiple sets of parameters to separately predict the liquid−liquid- and vapor−liquid-phase equilibria for hydrogen-bonding mixtures. This problem can be mitigated by separating the association (chemical) interactions from the physical dispersion and/or repulsion interactions in the NRTL model.[82,83] Moreover, the association interactions can be effectively predicted using perturbation theories[92] without knowing the association energy or the equilibrium constant of the "reaction"; technically, the association interactions are approximated by perturbation expansions from a reference fluid. Here, we follow the approach outlined in a recently published association-NRTL (A-NRTL) activity coefficient model[82] to improve the interpretation of the additive physical and chemical interactions in the synergistic coamorphous systems

$$\ln \gamma_i = \ln \gamma_i^{NRTL} + \ln \gamma_i^{Asso} \tag{13}$$

where $\ln \gamma_i^{NRTL}$ accounts for the physical force and is expressed using eq 11 but with different sets of $\tau_{ij}$; $\ln \gamma_i^{Asso}$ accounts for hydrogen-bonding or similar association interactions and is


https://doi.org/10.1021/acs.molpharmaceut.1c00353
Mol. Pharmaceutics XXXX, XXX, XXX−XXX

expressed using a simplified model[93] of the statistical associating fluid theory (SAFT)[94] that originates from Wertheim's thermodynamic perturbation theory.[95,96] According to Hao and Chen,[82] the overall association interaction is reflected by the concentration of unbonded hydrogen bond acceptor and donor sites in the mixture ($X^B$) and in the pure component ($X_i^B$)

$$\ln \gamma_i^{Asso} = \sum_B \nu_{B,i}\left[\ln\left(\frac{X^B}{X_i^B}\right) + \frac{X_i^B - 1}{2}\right] + r_i \sum_B \rho_B\left(\frac{1 - X^B}{2}\right) \quad (14)$$

Here, B denotes hydrogen bond acceptor (A) and donor (D) sites among all species; $\nu_{B,i}$ is the number of the B site in molecule $i$; $r_i$ is the normalized van der Waals volume of molecule $i$; and $\rho_B$ $(=\frac{\sum \nu_{B,i}X_i}{\sum r_i X_i})$ is the dimensionless molar density of the B site in the mixture. $X^B$ and $X_i^B$ are in units of mole fraction and are obtained from the mass balance

$$X^A = \frac{1}{1 + \sum_D \rho_D \Delta^{AD} X^D} \text{ and } X^D = \frac{1}{1 + \sum_A \rho_A \Delta^{AD} X^A} \quad (15)$$

and

$$X_i^A = \frac{1}{1 + \sum_{D,i} \rho_{D,i} \Delta^{AD} X_i^D} \text{ and } X_i^D = \frac{1}{1 + \sum_{A,i} \rho_{A,i} \Delta^{AD} X_i^A} \quad (16)$$

Here, $\rho_{B,i}$ $(=\frac{\nu_{B,i}}{r_i})$ is the dimensionless molar density of the B site in pure component $i$; and $\Delta^{AD}$ is the normalized association strength between an acceptor site and a donor site and is approximated by a product of the association strength parameters, $\delta^A$ and $\delta^D$, respectively, for the acceptor site and donor site, relative to a normalized reference association strength $\left(\frac{\Delta_{ref}^{AD}}{\delta_{ref}^A \delta_{ref}^D}\right)$

$$\Delta^{AD} = \frac{\delta^A \delta^D}{\delta_{ref}^A \delta_{ref}^D} \Delta_{ref}^{AD} \quad (17)$$

Moreover, $\Delta_{ref}^{AD}$ is chosen as that of the self-association in water molecules, as is recommended in the A-NRTL model, giving that $\delta_{ref}^A = 1$ and $\delta_{ref}^D = 1$, and

$$\Delta_{ref}^{AD} = 0.034\left[\exp\left(\frac{1960}{T}\right) - 1\right] \quad (18)$$

In the present study, $r_i$ is estimated by Bondi's group-contribution method.[97] $\nu_{B,i}$ is the number of acceptor and donor sites for each species as obtained from the PubChem database.[98−103] Furthermore, for a given species, all acceptor sites have the same $\delta^A$ and the same is true for donor sites. $\delta^A$, $\delta^D$, $\tau_{12}$, and $\tau_{21}$ are determined from the best fit to the $T_g$ data.

In what follows, we compare the two-parameter Margules (eq 9), NRTL (eqs 11 and 12), A-NRTL (eqs 13−18), and three-suffix Redlich−Kister (eq 10) activity coefficient models with the Gordon−Taylor (eq 1), Kovacs−Braun (eq 4), and Kwei (eq 3) equations in their description of the synergistic $T_g$ data for four binary pharmaceutical coamorphous mixtures: indomethacin−glibenclamide, indomethacin−arginine, acetaminophen−indomethacin, and fenretinide−cholic acid. The $k$ values used in this work are shown in Table 1. They are estimated using eq 6 along with experimental values of $\Delta C_{Pi}$ (per mole) for three of the four systems studied; for the system indomethacin/arginine, the $k$ value is taken from ref 31 and converted from a per-gram to per-mole basis. All adjustable parameters are determined from the best prediction of the composition-dependent $T_g$ data using the gradient descent method.[104] The uncertainties in the parameters are estimated from a biased error of ±5% on the $T_g$ data.

**Table 1. List of Sources and Values of $k$**

| coamorphous drug | source | value |
|---|---|---|
| indomethacin−glibenclamide | measured in this study | 1.37 |
| indomethacin−arginine | retrieved from ref 31 | 0.469[a] |
| acetaminophen−indomethacin | measured in this study | 1.39 |
| fenretinide−cholic acid | measured in this study | 1.11 |

[a]In ref 31, $k$ is determined as $T_{g1}/T_{g2}$ for a gram-based unit, and it is converted in this work to a per-mole basis.

**Materials.** Indomethacin (≥99%), glibenclamide (≥99%), acetaminophen (≥99%), and cholic acid (≥99%) are used as obtained from Sigma-Aldrich (St. Louis, MO) for the investigation. Fenretinide (≥98%) is obtained from Apexbio (Houston, TX) and used for the composition dependence study, whereas fenretinide (≥99%, Sigma-Aldrich) is used to measure the thermal properties of the pure compound. All materials were received and initially used in the crystalline state and tested by differential scanning calorimetry (DSC) to obtain the $T_g$ data. To compare the data measured in this study to that in the literature, data for indomethacin−glibenclamide and acetaminophen−indomethacin systems are also obtained from Pajula et al.[105] Data for the indomethacin−arginine system are taken from Jensen et al.[31] The chemical structure of the pharmaceutical molecules and other excipients that are studied here are provided in Table 2.

**Differential Scanning Calorimetry (DSC) Measurements and Analysis.** A conventional DSC (Mettler Toledo DSC 823e, Switzerland), equipped with a Freon cooling system and a nitrogen purge, was used to measure $T_g$, $T_m$ (melting point), and $\Delta C_{Pi}$ for all pure compounds and for the coamorphous mixtures as a function of composition. Prior to measurements, the DSC temperature and heat flow were calibrated using indium. Samples were sealed in 20 μL aluminum hermetic pans under nitrogen with sample mass ranging from 2 to 5 mg.

All DSC measurements included two heating cycles. Samples were first heated at 10 K/min from room temperature to 10 K above the $T_m$ of the pure glibenclamide, indomethacin, and cholic acid for the indomethacin−glibenclamide, acetaminophen−indomethacin, and fenretinide−cholic acid samples, respectively, followed by an isothermal hold for 1 min. Samples were then cooled at 10 K/min to 40 K below the $T_g$ of the pure indomethacin, acetaminophen, and fenretinide for the indomethacin−glibenclamide, acetaminophen−indomethacin, and fenretinide−cholic acid samples, respectively, with no recrystallization observed during cooling. A second heating scan was then performed at 10 K/min to 10 K above $T_m$, and $T_g$ was obtained on this scan. None of the scans showed an endotherm or exotherm at high temperatures related to degradation or decomposition. The scans also did not show any melting endotherms on the second heating and, thus, indicate the complete coamorph formation.

The melting points, $T_m$, for the pure compounds were obtained from the onset temperature of the melting


https://doi.org/10.1021/acs.molpharmaceut.1c00353
Mol. Pharmaceutics XXXX, XXX, XXX−XXX

**Table 2. Chemical Structures for Pharmaceutical Molecules and Excipients Investigated**

| | |
|---|---|
| Indomethacin | 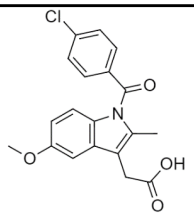 |
| Glibenclamide | 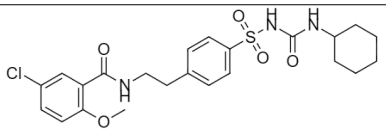 |
| Arginine | 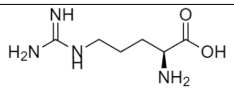 |
| Acetaminophen | 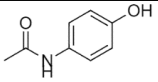 |
| Fenretinide | 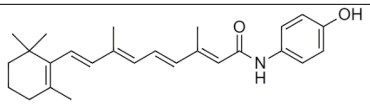 |
| Cholic Acid | 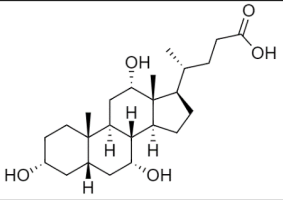 |

endotherms, and the results are provided in Table 3. $T_g$ values of the pure materials are obtained on the second heating by determining the fictive temperature, $T_f$,[106] using Moynihan's method,[107] and they are also provided in Table 3. $T_f$, measured on heating after cooling at a given rate in the absence of isothermal aging in the glassy state, is equivalent to $T_g$[108,109] measured on a cooling at that same rate; $T_f$ also represents the vitrified structure, where the glassy enthalpy intersects the extrapolated supercooled liquid enthalpy in a plot of enthalpy versus temperature. The DSC heat flow data for the second heating of the pure compounds are shown in Figure 1, where overshoots are obviously observed such that Moynihan's method is needed for a consistent analysis. However, since many researchers analyze such data using the midpoint method and ignoring the overshoot, we also provide midpoint $T_g$ values in Table 3 to compare with those from Moynihan's method. The $T_f$ values from Moynihan's method are lower than those from the midpoint method by as little as 0.6 °C for fenretinide to as much as 3.0 °C for glibenclamide; the difference is related to the magnitude of the overshoot relative to the significance of the step change $\Delta C_P$ at $T_g$, the latter of which is calculated at $T_f$ and is also provided in Table 3. In the current study, the $T_f$ values are used and referred to as $T_g$ for further modeling.

**Table 3. DSC Results of $T_{mi}$, $T_{fi}$, $T_{gi}$, and $\Delta C_{Pi}$ for Pure Indomethacin, Glibenclamide, Acetaminophen, Cholic Acid, and Fenretinide**

| $i$ | $T_{mi}$ (°C) | $T_{fi}$ (°C)[a] | $T_{gi}$ (°C)[b] | $\Delta C_{Pi}$ (J mol$^{-1}$ K$^{-1}$)[c] |
|---|---|---|---|---|
| indomethacin | 160.1 | 38.7 | 41.5 | 142.0 |
| glibenclamide | 168.8 | 52.5 | 55.5 | 194.6 |
| acetaminophen | 169.3 | 17.1 | 20.0 | 101.8 |
| cholic acid | 201.4 | 123.0 | 125.1 | 193.7 |
| fenretinide | 155.2 | 77.7 | 78.3 | 177.4 |

[a]$T_f$ is obtained using Moynihan's method.[107] [b]$T_g$ is obtained using the midpoint method. [c]$\Delta C_P$ is obtained at the corresponding $T_f$.

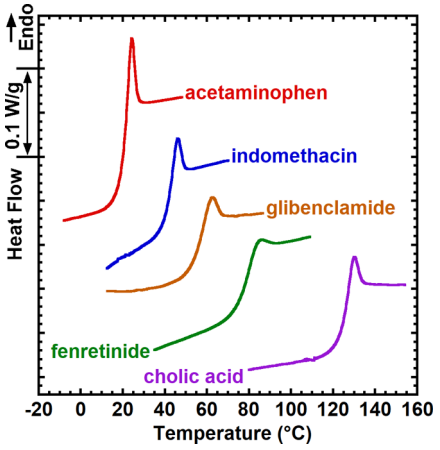


**Figure 1.** DSC heat flow data for pure acetaminophen, indomethacin, glibenclamide, fenretinide, and cholic acid measured on the second heating scan at 10 K/min.

## RESULTS

Experimental $T_g$ data for indomethacin(1)−glibenclamide(2) obtained in the present work (crosses) are shown in Figure 2A, along with the data from Pajula et al.[105] (open circles) and model predictions. For this coamorphous pharmaceutical mixture, the $T_g$ data manifest a maximum in the glibencla-


https://doi.org/10.1021/acs.molpharmaceut.1c00353
Mol. Pharmaceutics XXXX, XXX, XXX−XXX

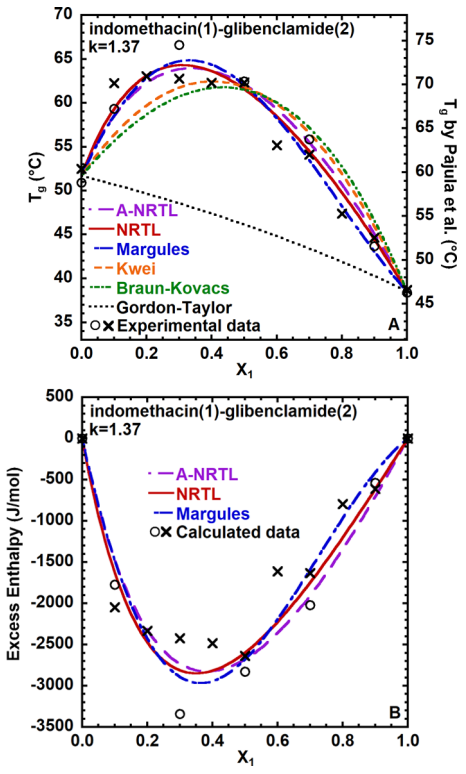


**Figure 2.** (A) $T_g$ data and model predictions for indomethacin(1)−glibenclamide(2) as a function of mole fraction indomethacin ($X_1$). The $T_g$ data measured in the present study (crosses) are plotted with respect to the left *y*-axis. The $T_g$ data obtained from Pajula et al.[105] (open circles) are plotted with respect to the right *y*-axis, which is shifted downwards, 7.9 °C relative to the left *y*-axis. All model predictions are plotted with respect to the left *y*-axis as well. (B) Excess enthalpy for indomethacin(1)−glibenclamide(2) as a function of $X_1$ calculated from experimental data using eq 5 and predicted by activity coefficient models, with symbols as in (A).

mide-rich region near $X_1$ = 0.30, 14−18 °C above the Gordon−Taylor prediction. The two sets of experimental data are consistent with one another with respect to the composition dependence, although the $T_g$ data measured by Pajula et al. are on average 7.9 °C higher than our data, as is indicated by the secondary *y*-axis in Figure 2A. The difference is presumably due to the fact that Pajula et al. cooled their samples at an uncontrolled and faster rate resulting in a higher $T_g$,[108] and they took the midpoint $T_g$ rather than using the $T_f$ from Moynihan's method, which also increases $T_g$ by roughly 3 °C. The $T_g$ data measured in the present study and the shifted data from Pajula et al. were fitted to eq 5, with $\Delta H^E_{liq}$ given by the A-NRTL, NRTL, and two-parameter Margules activity coefficient models and with the *k* value, which is equated to the ratio of $\Delta C_{P2}/\Delta C_{P1}$ in eq 6, experimentally found here to be 1.37. The adjustable parameter values, along with the root-mean-square error (RMSE) from the model fits to the $T_g$ data, are reported in Table 4. For the A-NRTL model, the values of $r_i$, $\nu_i^B$, $\delta^A$, and $\delta^D$ parameters are reported in Table 5; of particular note, the $\delta^A$ and $\delta^D$ values for indomethacin were optimized by simultaneously fitting the $T_g$ data for the three coamorphous systems that contain indomethacin. The A-NRTL, NRTL, and two-parameter Margules models all quantitatively predict the off-center maximum $T_g$ near $X_1$ = 0.30 and its magnitude, giving RMSE values of 1.4−1.8 °C. The activity coefficient model parameters are further used to calculate $\Delta H^E_{liq}$ based on eqs 10, 11, and 13, with the predictions of $\Delta H^E_{liq}$ plotted in Figure 2B against mole fraction indomethacin. Also shown as points are $\Delta H^E_{liq}$ data calculated from eq 5 using the $T_g$ data. The A-NRTL, NRTL, and Margules models predict negative bell-shaped curves that agree well with the data and indicate the miscibility between the two species in the liquid state. The fits of the Kwei and Braun−Kovacs equations are also shown in Figure 2A using the experimental *k* value of 1.37, and both models predict a maximum close to the equimolar composition rather than the observed asymmetric data, resulting in larger RMSE values of 2.8 and 3.3 °C, respectively.

Experimental $T_g$ data for indomethacin(1)−arginine(2) from Jensen et al.[31] are shown in Figure 3A, along with model predictions. The corresponding excess enthalpy plots are shown in Figure 3B. For this coamorphous pharmaceutical

**Table 4. Values of Fitting Parameters and Mean-Square Errors for the Four Pharmaceutical Coamorphous Systems Investigated**

| | indomethacin(1)−glibenclamide(2) | indomethacin(1)−arginine(2) | acetaminophen(1)−indomethacin(2) | fenretinide(1)−cholic acid(2) |
|---|---|---|---|---|
| | | A-NRTL | | |
| $\tau_{12}$ | −3.21 ± 0.24 | −1.49 ± 0.44 | −1.52 ± 0.23 | −1.10 ± 0.66 |
| $\tau_{21}$ | 2.13 ± 0.88 | 0.362 ± 0.80 | 2.81 ± 0.86 | 6.76 ± 4.30 |
| RMSE (°C) | 1.76 | 5.01 | 0.82 | 4.25 |
| | | NRTL | | |
| $\tau_{12}$ | −3.54 ± 0.23 | −2.44 ± 0.34 | −1.72 ± 0.22 | −2.03 ± 0.53 |
| $\tau_{21}$ | 2.28 ± 0.94 | −2.88 ± 0.35 | 3.54 ± 1.22 | 8.33 ± 4.50 |
| RMSE (°C) | 1.44 | 5.77 | 0.73 | 5.70 |
| | | Margules | | |
| $A'_{12}$ | −6.48 ± 0.96 | −7.07 ± 1.03 | 0.187 ± 0.663 | 3.46 ± 1.63 |
| $A'_{21}$ | −1.20 ± 0.92 | −8.10 ± 1.22 | −0.755 ± 0.626 | −6.05 ± 1.61 |
| RMSE (°C) | 1.62 | 5.57 | 0.80 | 2.94 |
| | | Kwei | | |
| *q* (°C) | 62.7 ± 7.2 | 227 ± 18 | 6.16 ± 6.76 | 25.9 ± 13.8 |
| RMSE (°C) | 2.76 | 8.41 | 0.95 | 6.02 |
| | | Braun−Kovacs | | |
| *q* (°C) | 72.8 ± 8.3 | 163 ± 13 | 7.62 ± 8.05 | 28.1 ± 14.5 |
| RMSE (°C) | 3.29 | 6.53 | 0.92 | 5.93 |


https://doi.org/10.1021/acs.molpharmaceut.1c00353
Mol. Pharmaceutics XXXX, XXX, XXX−XXX

**Table 5. Values of A-NRTL Parameters $r_i$, $\nu_{B,i}$, and $\delta^B$ for Species Studied Here**

| $i$ | $r_i$ | $\nu_{A,i}$ | $\nu_{D,i}$ | $\delta^A$ | $\delta^D$ |
|---|---|---|---|---|---|
| indomethacin[a] | 12.1 | 4 | 1 | 4.17 ± 0.36 | 1.33 ± 0.31 |
| glibenclamide | 17.1 | 5 | 3 | 4.09 ± 0.57 | 3.97 ± 0.25 |
| arginine | 6.45 | 4 | 4 | 0.75 ± 0.15 | 8.54 ± 1.17 |
| acetaminophen | 5.60 | 2 | 2 | 6.05 ± 0.70 | 0.21 ± 0.09 |
| cholic acid | 17.5 | 5 | 4 | 1.09 ± 0.41 | 4.52 ± 3.80 |
| fenretinide | 16.1 | 2 | 2 | 4.98 ± 2.64 | 0.11 ± 0.60 |

[a]For indomethacin, values of $\delta^A$ and $\delta^D$ are obtained by simultaneously fitting the $T_g$ data for three systems, indomethacin−glibenclamide, indomethacin−arginine, and acetaminophen−indomethacin.

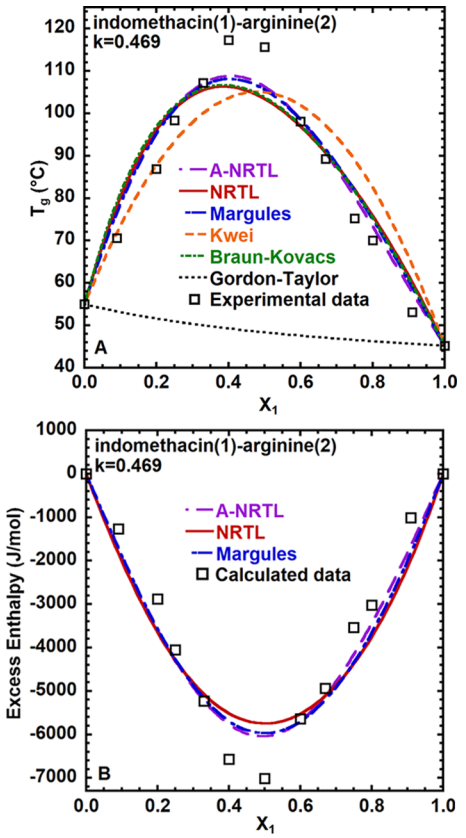


**Figure 3.** (A) $T_g$ data and model predictions for indomethacin(1)−arginine(2) as a function of mole fraction indomethacin ($X_1$). The $T_g$ data are obtained from Jensen et al.[31] (B) Excess enthalpy for indomethacin(1)−arginine(2) as a function of $X_1$ calculated from experimental data using eq 5 and predicted by activity coefficient models.

mixture, the $T_g$ data manifest a maximum near $X_1$ = 0.45, 69 °C above the Gordon−Taylor prediction, which is 7 times higher than $T_{g2} - T_{g1}$. The composition dependence, indicated as the slope of $dT_g/dX_1$, gradually strengthens when approaching the maximum. The $T_g$ data measured by Jensen et al. were fitted to the activity coefficient models using the experimental $k$ value of 0.469, which is approximated (for units of per gram) by $T_{g1}/T_{g2}$[31] and then further normalized by us by the ratio of the molecular weights to convert the units from per gram to per mole. The model parameters, along with the RMSE values for the fits to the data, are reported in Table 4, and the A-NRTL model parameters are reported in Table 5. The A-NRTL, NRTL, and two-parameter Margules models qualitatively predict a maximum $T_g$ near $X_1$ = 0.45, but its magnitude is underestimated and the gradually increasing $dT_g/dX_1$ when approaching the maximum is not captured. The RMSE values for all three models are over 5 °C, although the fit of the A-NRTL model is slightly better than the other two. The A-NRTL, NRTL, and Margules models also predict negative bell-shaped curves of $\Delta H^E_{liq}$ versus composition that qualitatively agree with the data, as shown in Figure 3B, indicating the miscibility between two species in the liquid state, but the magnitude of the minimum is not captured. The fits of the Kwei and Braun−Kovacs equations are also shown in Figure 3A using the experimental $k$ value of 0.469; neither are satisfactory, giving RMSE values of 8.4 and 6.5 °C, respectively.

Experimental $T_g$ data for acetaminophen(1)−indomethacin(2) obtained in the present work (crosses) are shown in Figure 4A, along with the data from Pajula et al.'s[105] (open circles) and model predictions. The corresponding excess enthalpy plots are shown in Figure 4B. For this coamorphous pharmaceutical mixture, the $T_g$ data manifest a monotonically descending inflectional behavior, showing a gradually diminished negative $dT_g/dX_1$ followed by a gradually strengthened one, with the inflection point located in the acetaminophen-rich region near $X_1$ = 0.30. The two sets of experimental data

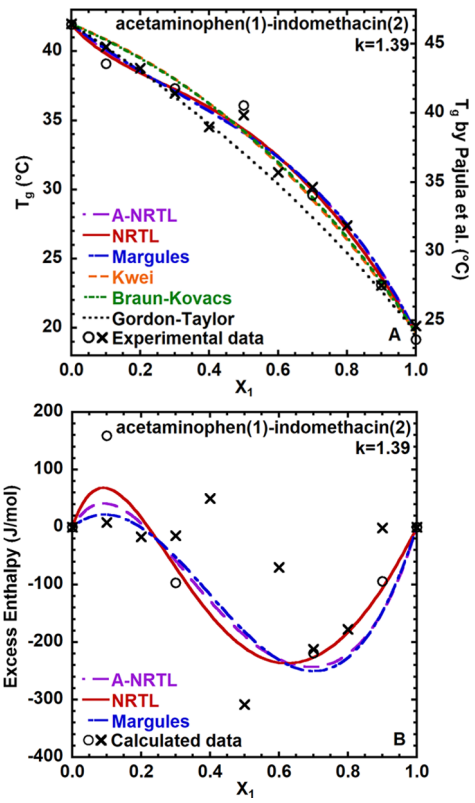


**Figure 4.** (A) $T_g$ data and model predictions for acetaminophen(1)−indomethacin(2) as a function of mole fraction acetaminophen ($X_1$). The $T_g$ data measured in the present study (crosses) are plotted with respect to the left $y$-axis. The $T_g$ data obtained from Pajula et al.[105] (open circles) are plotted with respect to the right $y$-axis, which is shifted downwards, 4.5 °C relative to the left $y$-axis. All model predictions are plotted with respect to the left $y$-axis as well. (B) Excess enthalpy for acetaminophen(1)−indomethacin(2) as a function of $X_1$ calculated from experimental data using eq 5 and predicted by activity coefficient models, with symbols as in (A).


https://doi.org/10.1021/acs.molpharmaceut.1c00353
Mol. Pharmaceutics XXXX, XXX, XXX−XXX

are consistent with one another with respect to the composition dependence, although the $T_g$ data measured by Pajula et al. are on average 4.5 °C higher than our data, as is indicated by the secondary $y$-axis in Figure 4A, due to their higher cooling rate and midpoint analysis method as described above for the indomethacin−glibenclamide system. The $T_g$ data measured in the present study and the shifted data from Pajula et al. were fitted to the activity coefficient models using an experimental $k$ value of 1.39. The model parameters, along with the RMSE values for the fits to the data, are reported in Table 4, and the A-NRTL model parameters are reported in Table 5. The A-NRTL, NRTL, and two-parameter Margules models all quantitatively predict the inflection point near $X_1$ = 0.30 and its curvature, giving RMSE values of 0.7−0.8 °C. In Figure 4B, the A-NRTL, NRTL, and Margules models predict an "unlike" (positive $\Delta H^E_{liq}$ maximum) interaction in the indomethacin-rich region followed by a "like" (negative $\Delta H^E_{liq}$ minimum) interaction that qualitatively agrees with the data. The fits of the Kwei and Braun−Kovacs equations are also shown in Figure 4A using an experimental $k$ value of 1.39, and neither predict the observed inflectional behavior.

Experimental $T_g$ data for fenretinide(1)−cholic acid(2) obtained in the present work are shown in Figure 5A, along with model predictions. The corresponding excess enthalpy plots are shown in Figure 5B. For this coamorphous pharmaceutical mixture, the $T_g$ data manifest a descending inflectional behavior similar to that of the acetaminophen−indomethacin system, except that the inflection point is located in the cholic acid-rich region near $X_1$ = 0.65, and for $X_1$ > 0.80, the gradually strengthened negative $dT_g/dX_1$ is much stronger than is observed for acetaminophen−indomethacin, leading to an elevation of $T_g$ 14 °C above the Gordon−Taylor prediction. The $T_g$ data measured in the present study were fitted to the activity coefficient models using an experimental $k$ value of 1.11. The model parameters, along with the RMSE values for the fits to the data, are reported in Table 4, and the A-NRTL model parameters are reported in Table 5. The best description of the inflectional behavior is given by the two-parameter Margules model with an RMSE value of 2.9 °C. The A-NRTL and NRTL models do not capture the location of the inflection point, although the A-NRTL model improves the correlation of the NRTL model with the prediction of the inflection point right-shifted from $X_1$ = 0.20 to 0.30.

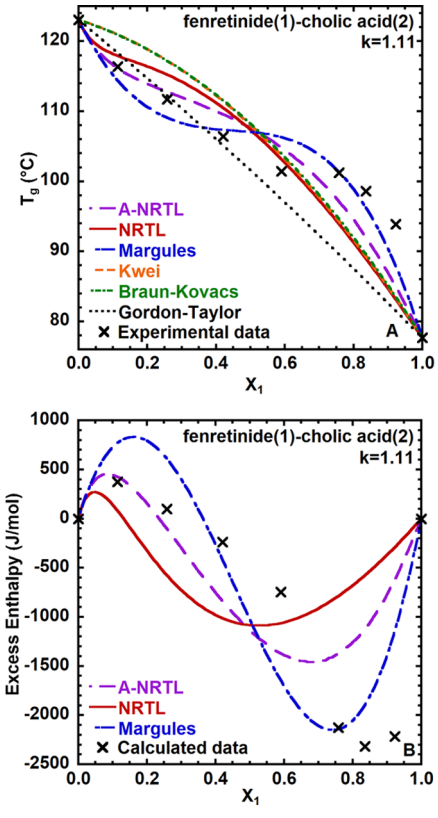


**Figure 5.** (A) $T_g$ data measured in the present study and model predictions for fenretinide(1)−cholic acid(2) as a function of mole fraction fenretinide ($X_1$). (B) Excess enthalpy for fenretinide(1)−cholic acid(2) as a function of $X_1$ calculated from experimental data using eq 5 and predicted by activity coefficient models.

In Figure 5B, although all three of these activity coefficient models predict unlike (positive $\Delta H^E_{liq}$ maximum) interactions in the cholic acid-rich region followed by the like (negative $\Delta H^E_{liq}$ minimum) interaction in the fenretinide-rich region, none quantitatively describe the strength or position of the strong like interaction. Again, the two-parameter Margules model gives the closest description of this $\Delta H^E_{liq}$, predicting a minimum of −2100 J/mol near $X_1$ = 0.75, compared to an experimental minimum of −2300 J/mol at $X_1$ = 0.85. The fits of the Kwei and Braun−Kovacs equations are also shown in Figure 5A using an experimental $k$ value of 1.11, and neither predict the observed inflectional behavior.

## DISCUSSION

Examination of the $\tau_{ij}$ parameters for NRTL and A-NRTL models shows that the $\tau_{ij}$ values are generally of smaller magnitude but the same sign for A-NRTL in comparison to those for NRTL. This is because the $\tau_{ij}$ terms in A-NRTL only account for the physical dispersion and/or repulsion and not for the chemical association interactions. A similar result was observed by Hao and Chen.[82] However, in the case of the indomethacin−arginine system, the sign of $\tau_{21}$ changes from the negative for NRTL to the positive for A-NRTL, as shown in Table 4. This change of the sign is due to the flexibility of this parameter in terms of its contribution to the overall interactions, given that the majority of the like interactions are captured by the statistical association theory in A-NRTL, i.e., 90% of $\Delta H^E_{liq}$ is attributed to the summation of $X_i\gamma_i^{Asso}$.

Furthermore, values of the $\delta^A$ and $\delta^D$ parameters in A-NRTL qualitatively reveal information concerning the sites of the association interactions. For indomethacin and glibenclamide, the values of $\delta^A$ are 4.17 and 4.09, respectively, indicating comparable strong associating abilities of the acceptor site toward the donor site for both species; the $\delta^D$ parameter value for glibenclamide is 3.97 and is 3 times higher than that for indomethacin. Hence, a competition exists between the self-association within glibenclamide and the cross-association between the two species, leading to a weak net association interaction. Thus, magnitudes of the $\tau_{ij}$ parameters for A-NRTL are only slightly reduced in comparison to those for NRTL. Similarly, for acetaminophen−indomethacin, competition between the self- and cross-associations exists, and the result is a weak net association interaction.

On the other hand, for indomethacin−arginine, values of the $\delta^A$ and $\delta^D$ parameters indicate a strong cross-association between the acceptor site in indomethacin and the donor site in arginine, which is consistent with strong interactions between the indomethacin carboxylate group and the arginine


https://doi.org/10.1021/acs.molpharmaceut.1c00353
Mol. Pharmaceutics XXXX, XXX, XXX−XXX

guanidine group, as observed by Jensen et al.[31] using Fourier transform infrared (FTIR) spectroscopy. However, the statistical association-NRTL model does not well describe the gradually strengthened $dT_g/dX_1$ when approaching the maximum $T_g$ due to two potential reasons. First, $\Delta^{AD}$ is not a constant parameter but is assumed to decrease as temperature increases, being proportional to $1/T$ in eq 18; eliminating this constraint in the model and allowing $\Delta^{AD}$ to be independent of temperature result in an improved fit that qualitatively captures the gradually steepened slope giving an RMSE value of 3.0 °C. A second potential issue is that each site is assumed to establish only one single association with another site[92] and all acceptor and donor sites on a given molecule are assumed to be identical. Thus, a model that can describe more complex and higher-order interactions, such as the three-suffix Redlich–Kister activity coefficient model,[86] eq 10, provides a quantitative description of both $T_g$ and $\Delta H^E_{liq}$, as shown in Figure 6, where both the gradually steepened slope and the level of the maximum $T_g$ are captured, giving an RMSE value of 2.1 °C; the three-suffix Redlich–Kister model also uses an experimental $k$ value of 0.47, and values of the $B_{12}$, $C_{12}$, and $D_{12}$ fitting parameters are −8.34, 0.27, and 5.91, respectively.

For fenretinide–cholic acid, values of the $\delta^A$ and $\delta^D$ parameters also indicate a strong cross-association between the acceptor site in fenretinide and the donor site in cholic acid. The association interaction is extremely strong for $X_1 > 0.70$, as is manifested by the positive deviation of $T_g$ that is 11.8 °C above the Gordon–Taylor prediction at $X_1 = 0.76$ and is equivalent to 31% of the $T_g$ data range. Neither the NRTL nor the A-NRTL models predict strong like interactions in this range. On the other hand, the three-suffix Redlich–Kister model can again capture this large positive deviation, as is also shown in Figure 6, giving an RMSE of 1.6 °C, implying the existence of more complex or higher-order interactions in the fenretinide-rich region; the three-suffix Redlich–Kister model also uses an experimental $k$ value of 1.11, and values of the $B_{12}$, $C_{12}$, and $D_{12}$ fitting parameters are −0.42, −4.31, and −5.11, respectively.

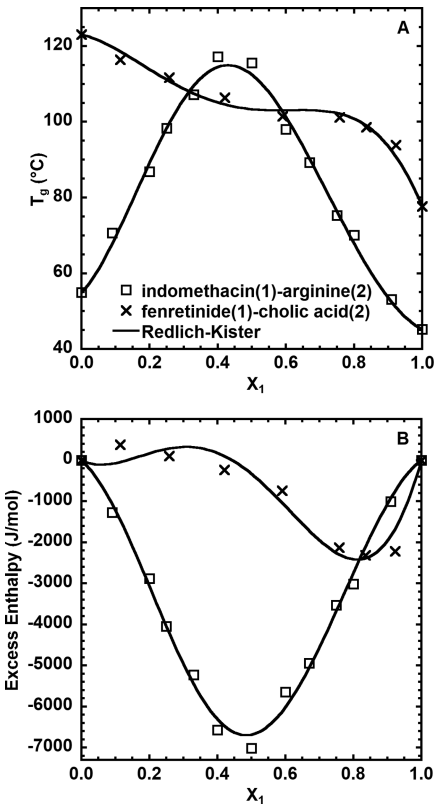


**Figure 6.** (A) $T_g$ data and the three-suffix Redlich–Kister activity coefficient model predictions for indomethacin(1)–arginine(2) (open squares) and fenretinide(1)–cholic acid(2) (crosses). (B) Excess enthalpy data for the same system calculated from experimental data using eq 5 and predictions of the three-suffix Redlich–Kister activity coefficient models.

As was pointed out in the Introduction section, the Kwei and Braun–Kovacs equations are often able to describe the $T_g$ data when $k$ is taken as a fitting parameter. In fact, Kwei[49] applied the equation to describe inflectional behavior for the mixture of poly(methyl methacrylate) and Novolac B with $k$ equal to 12, compared to an experimental $k$ value of 0.94 (estimated by $T_{g1}/T_{g2}$). Similarly, in this work, the Kwei equation, eq 3, quantitatively captures the inflectional $T_g$ data for acetaminophen–indomethacin, with $k$ and $q$ equal to 0.35 ± 0.11 and 35.6 ± 6.8 °C, respectively, giving an RMSE value of 0.74 °C; in addition, the Kwei equation can quantitatively capture the inflectional $T_g$ for fenretinide–cholic acid, with $k$ and $q$ equal to 9.2 ± 3.3 and −57.0 ± 13.7 °C, respectively, giving an RMSE value of 0.76 °C. However, the Kwei equation cannot describe the synergistic off-center maximum $T_g$ for indomethacin–glibenclamide even when $k$ is taken as a fitting parameter because the term $qw_1w_2$, in eq 3, always favors an extremum at $w_1 = 0.50$ or $X_1 = 0.60$, rather than at the experimentally observed value of $w_1 = 0.25$ or $X_1 = 0.30$. On the other hand, the Braun–Kovacs equation, eq 4, quantitatively captures the off-center maximum of $T_g$ for indomethacin–glibenclamide, with $k$ and $q$ equal to 0.32 ± 0.12 and 51.2 ± 4.9 °C, respectively, giving an RMSE value of 1.4 °C. However, the Braun–Kovacs equation cannot describe inflectional $T_g$ data. Thus, both the Kwei and Braun–Kovacs equations have significant limitations in describing the composition dependence of $T_g$ for coamorphous systems with strong interactions, even when $k$ is taken as a fitting parameter. Furthermore, when $k$ is adjusted, the physical meaning is lost and the equations do not provide the insight needed to understand and predict coamorphous systems.

Importantly, our methodology uses a $k$ parameter equal to the experimental value of $\Delta C_{P2}/\Delta C_{P1}$ and, thus, the appropriate physics is captured, allowing synergistic $T_g$ behaviors to not only be described but also be predicted if activity model parameters can be determined from other data or simulations. In fact, activity coefficient models have been widely used to solve solid–liquid equilibrium problems to predict the aqueous solubility[84,110,111] of pharmaceutical molecules and the miscibility[105,112,113] between coamorphous or cocrystal species. In addition, activity coefficient model parameters can be obtained directly from molecular dynamics simulations[114,115] or can be predetermined by correlating solid–liquid equilibria data in simple liquids, for example, using the UNIFAC,[116] NRTL-segment activity coefficient (SAC),[117,118] or association-NRTL-SAC.[119] The NRTL-SAC model has been used to predict drug solubility in complex solvents,[120−122] and it focuses on the characteristic hydrophobicity, hydrophilicity, and polar attractivity and repulsivity of single molecules, sophisticatedly accounting for the overall intermolecular interactions, which can be obtained by fitting equilibria data for simple molecular liquids. The association-


https://doi.org/10.1021/acs.molpharmaceut.1c00353
Mol. Pharmaceutics XXXX, XXX, XXX−XXX

NRTL-SAC model shares similar advantages and improves the description for association interactions. The NRTL-SAC and association-NRTL-SAC models are anticipated to be useful, with parameters predetermined from the simple phase equilibria data, for developing an entirely predictive approach to guide the discovery and development of stable coamorphous pharmaceutical materials. To the best of our knowledge, the connection between thermodynamic properties and the synergistic $T_g$ data has not been previously made for pharmaceutical coamorphous glasses. Moreover, pharmaceutical coamorphs are currently discovered using a trial-and-error process that is inefficient and costly, and predictive methods are needed to guide the discovery of new and useful coamorphous pharmaceuticals. From this perspective, our framework for modeling $T_g$ as a function of composition using activity coefficient models provides a methodology to bridge these gaps.

## CONCLUSIONS

The synergistic glass transition temperature ($T_g$) of binary pharmaceutical coamorphous mixtures is well described by extending Couchman and Karasz's approach and using activity coefficient models for the excess enthalpy in the liquid state. The off-center maximum in $T_g$ data as a function of composition is captured by the A-NRTL, NRTL, and two-parameter Margules models, quantitatively for indomethacin−glibenclamide and qualitatively for indomethacin−arginine. The inflectional $T_g$ behavior for acetaminophen−indomethacin is quantitatively predicted by these three-activity coefficient models, whereas that for fenretinide−cholic acid is poorly captured due to the insufficient description of the strong like interaction in the fenretinide-rich region. The three-suffix Redlich−Kister activity model quantitatively describes the nonideality for indomethacin−arginine and fenretinide−cholic acid indicating complex binary or higher-order associations. Our methodology assumes that the $k$ parameter in the $T_g$ versus composition equations is equal to the experimental value of $\Delta C_{P2}/\Delta C_{P1}$. On the other hand, the Kwei and Braun−Kovacs equations can capture only the inflectional or asymmetrical maximum behavior, respectively, when $k$ is treated as a fitting parameter, and in this situation, $k$ loses its physical significance. The framework developed here is anticipated to be able to be extended to allow predictions of $T_g$ and miscibility of coamorphous mixtures using activity coefficient models with parameters obtained from solubility data and/or molecular simulations.

## AUTHOR INFORMATION


### Corresponding Author

**Sindee L. Simon** − *Department of Chemical Engineering, Texas Tech University, Lubbock, Texas 79409, United States; Department of Chemical and Biomolecular Engineering, North Carolina State University, Raleigh, North Carolina 27695, United States;* orcid.org/0000-0001-7498-2826; Email: slsimon@ncsu.edu

### Authors

**Xiao Zhao** − *Department of Chemical Engineering, Texas Tech University, Lubbock, Texas 79409, United States*

**Sixue Cheng** − *Department of Chemical Engineering, Texas Tech University, Lubbock, Texas 79409, United States*

**Yung P. Koh** − *Department of Chemical Engineering, Texas Tech University, Lubbock, Texas 79409, United States*

**Brandon D. Kelly** − *Department of Chemical Engineering, Texas Tech University, Lubbock, Texas 79409, United States*

**Gregory B. McKenna** − *Department of Chemical Engineering, Texas Tech University, Lubbock, Texas 79409, United States; Department of Chemical and Biomolecular Engineering, North Carolina State University, Raleigh, North Carolina 27695, United States;* orcid.org/0000-0002-5676-9930

Complete contact information is available at: https://pubs.acs.org/10.1021/acs.molpharmaceut.1c00353


### Notes

The authors declare no competing financial interest.

## ACKNOWLEDGMENTS

The authors gratefully acknowledge National Science Foundation under grants DMR-2004960 and CMMI-1662046. The authors thank Drs. Chau-Chyun Chen and Yifan Hao for help with the association-NRTL modeling.

## REFERENCES


(1) Clas, S.-D.; Cotton, M.; Moran, E.; Spagnoli, S.; Zografi, G.; Vadas, E. B. Assessment of the physical stability of lyophilized MK-0591 by differential scanning calorimetry. *Thermochim. Acta* **1996**, *288*, 83−96.

(2) DiNunzio, J. C.; Miller, D. A.; Yang, W.; McGinity, J. W.; Williams, R. O., III Amorphous compositions using concentration enhancing polymers for improved bioavailability of itraconazole. *Mol. Pharmaceutics* **2008**, *5*, 968−980.

(3) Aso, Y.; Yoshioka, S.; Kojima, S. Molecular mobility-based estimation of the crystallization rates of amorphous nifedipine and phenobarbital in poly (vinylpyrrolidone) solid dispersions. *J. Pharm. Sci.* **2004**, *93*, 384−391.

(4) Li, T. Materials engineering of solid-state dosage forms. *Pharm. Res.* **2008**, *25*, 949−952.

(5) Chokshi, R. J.; Shah, N. H.; Sandhu, H. K.; Malick, A. W.; Zia, H. Stabilization of low glass transition temperature indomethacin formulations: Impact of polymer-type and its concentration. *J. Pharm. Sci.* **2008**, *97*, 2286−2298.

(6) Zhou, D. L.; Grant, D. J. W.; Zhang, G. G. Z.; Law, D.; Schmitt, E. A. A calorimetric investigation of thermodynamic andmolecular mobility contributions to the physical stability of two pharmaceutical glasses. *J. Pharm. Sci.* **2007**, *96*, 71−83.

(7) Zhu, L.; Wong, L.; Yu, L. Surface-enhanced crystallization of amorphous nifedipine. *Mol. Pharmaceutics* **2008**, *5*, 921−926.

(8) Baird, J. A.; Van Eerdenbrugh, B.; Taylor, L. S. A classification system to assess the crystallization tendency of organic molecules from undercooled melts. *J. Pharm. Sci.* **2010**, *99*, 3787−3806.

(9) Yoshioka, S.; Aso, Y. Correlations between molecular mobility and chemical stability during storage of amorphous pharmaceuticals. *J. Pharm. Sci.* **2007**, *96*, 960−981.

(10) Wu, T.; Yu, L. Surface crystallization of indomethacin below $T_g$. *Pharm. Res.* **2006**, *23*, 2350−2355.

(11) Kothari, K.; Ragoonanan, V.; Suryanarayanan, R. The role of drug−polymer hydrogen bonding interactions on the molecular mobility and physical stability of nifedipine solid dispersions. *Mol. Pharmaceutics* **2015**, *12*, 162−170.

(12) Mistry, P.; Mohapatra, S.; Gopinath, T.; Vogt, F. G.; Suryanarayanan, R. Role of the strength of drug−polymer interactions on the molecular mobility and crystallization inhibition in ketoconazole solid dispersions. *Mol. Pharmaceutics* **2015**, *12*, 3339−3350.

(13) Maclean, J.; Medina, C.; Daurio, D.; Alvarez-Nunez, F.; Jona, J.; Munson, E.; Nagapudi, K. Manufacture and performance evaluation of a stable amorphous complex of an acidic drug molecule and neusilin. *J. Pharm. Sci.* **2011**, *100*, 3332−3344.

(14) Trasi, N. S.; Taylor, L. S. Nucleation and crystal growth of amorphous nilutamide−unusual low temperature behavior. *CrystEngComm* **2014**, *16*, 7186−7195.
(15) Sun, Y.; Zhu, L.; Wu, T.; Cai, T.; Gunn, E. M.; Yu, L. Stability of amorphous pharmaceutical solids: crystal growth mechanisms and effect of polymer additives. *AAPS J.* **2012**, *14*, 380−388.
(16) Chavan, R. B.; Thipparaboina, R.; Kumar, D.; Shastri, N. R. Co amorphous systems: A product development perspective. *Int. J. Pharm.* **2016**, *515*, 403−415.
(17) Laitinen, R.; Lobmann, K.; Strachan, C. J.; Grohganz, H.; Rades, T. Emerging trends in the stabilization of amorphous drugs. *Int. J. Pharm.* **2013**, *453*, 65−79.
(18) Dengale, S. J.; Grohganz, H.; Rades, T.; Löbmann, K. Recent advances in co-amorphous drug formulations. *Adv. Drug Delivery Rev.* **2016**, *100*, 116−125.
(19) Fung, M. H.; Suryanarayanan, R. Effect of organic acids on molecular mobility, physical stability, and dissolution of ternary ketoconazole spray-dried dispersions. *Mol. Pharmaceutics* **2019**, *16*, 41−48.
(20) Stepanov, V.; Patel, R. B.; Mudryy, R.; Qiu, H. W. Investigation of nitramine-based amorphous energetics. *Propellants, Explos., Pyrotech.* **2016**, *41*, 142−147.
(21) Shamim, N.; Koh, Y. P.; Simon, S. L.; McKenna, G. B. The glass transition of trinitrotoluene (TNT) by flash DSC. *Thermochim. Acta* **2015**, *620*, 36−39.
(22) Fung, M.; Bērziņš, K.; Suryanarayanan, R. Physical stability and dissolution behavior of ketoconazole−organic acid coamorphous systems. *Mol. Pharmaceutics* **2018**, *15*, 1862−1869.
(23) Fung, M. H.; DeVault, M.; Kuwata, K. T.; Suryanarayanan, R. Drug-excipient interactions: effect on molecular mobility and physical stability of ketoconazole−organic acid coamorphous systems. *Mol. Pharmaceutics* **2018**, *15*, 1052−1061.
(24) Löbmann, K.; Laitinen, R.; Grohganz, H.; Gordon, K. C.; Strachan, C.; Rades, T. Coamorphous drug systems: enhanced physical stability and dissolution rate of indomethacin and naproxen. *Mol. Pharmaceutics* **2011**, *8*, 1919−1928.
(25) Wu, W. Q.; Ueda, H.; Lobmann, K.; Rades, T.; Grohganz, H. Organic acids as co-formers for co-amorphous systems - Influence of variation in molar ratio on the physicochemical properties of the co-amorphous systems. *Eur. J. Pharm. Biopharm.* **2018**, *131*, 25−32.
(26) Wu, W. Q.; Löbmann, K.; Schnitzkewitz, J.; Knuhtsen, A.; Pedersen, D. S.; Grohganz, H.; Rades, T. Aspartame as a co-former in co-amorphous systems. *Int. J. Pharm.* **2018**, *549*, 380−387.
(27) Mishra, J.; Lobmann, K.; Grohganz, H.; Rades, T. Influence of preparation technique on co-amorphization of carvedilol with acidic amino acids. *Int. J. Pharm.* **2018**, *552*, 407−413.
(28) Kasten, G.; Grohganz, H.; Rades, T.; Löbmann, K. Development of a screening method for co-amorphous formulations of drugs and amino acids. *Eur. J. Pharm. Sci.* **2016**, *95*, 28−35.
(29) Kasten, G.; Nouri, K.; Grohganz, H.; Rades, T.; Löbmann, K. Performance comparison between crystalline and co-amorphous salts of indomethacin-lysine. *Int. J. Pharm.* **2017**, *533*, 138−144.
(30) Kasten, G.; Löbmann, K.; Grohganz, H.; Rades, T. Co-former selection for co-amorphous drug-amino acid formulations. *Int. J. Pharm.* **2019**, *557*, 366−373.
(31) Jensen, K. T.; Larsen, F. H.; Lobmann, K.; Rades, T.; Grohganz, H. Influence of variation in molar ratio on co-amorphous drug-amino acid systems. *Eur. J. Pharm. Biopharm.* **2016**, *107*, 32−39.
(32) Jensen, K. T.; Blaabjerg, L. I.; Lenz, E.; Bohr, A.; Grohganz, H.; Kleinebudde, P.; Rades, T.; Lobmann, K. Preparation and characterization of spray-dried co-amorphous drug-amino acid salts. *J. Pharm. Pharmacol.* **2016**, *68*, 615−624.
(33) Jensen, K. T.; Larsen, F. H.; Cornett, C.; Löbmann, K.; Grohganz, H.; Rades, T. Formation mechanism of coamorphous drug−amino acid mixtures. *Mol. Pharmaceutics* **2015**, *12*, 2484−2492.
(34) Lim, A. W.; Lobmann, K.; Grohganz, H.; Rades, T.; Chieng, N. Investigation of physical properties and stability of indomethacin-cimetidine and naproxen-cimetidine co-amorphous systems prepared by quench cooling, coprecipitation and ball milling. *J. Pharm. Pharmacol.* **2016**, *68*, 36−45.
(35) Mesallati, H.; Conroy, D.; Hudson, S.; Tajber, L. Preparation and characterization of amorphous ciprofloxacin-amino acid salts. *Eur. J. Pharm. Biopharm.* **2017**, *121*, 73−89.
(36) Gao, Y.; Liao, J.; Qi, X.; Zhang, J. J. Coamorphous repaglinide−saccharin with enhanced dissolution. *Int. J. Pharm.* **2013**, *450*, 290−295.
(37) Ueda, H.; Muranushi, N.; Sakuma, S.; Ida, Y.; Endoh, T.; Kadota, K.; Tozuka, Y. A strategy for co-former selection to design stable co-amorphous formations based on physicochemical properties of non-steroidal inflammatory drugs. *Pharm. Res.* **2016**, *33*, 1018−1029.
(38) Hu, Y.; Gniado, K.; Erxleben, A.; McArdle, P. Mechanochemical reaction of sulfathiazole with carboxylic acids: Formation of a cocrystal, a salt, and coamorphous solids. *Cryst. Growth Des.* **2014**, *14*, 803−813.
(39) Ojarinta, R.; Heikkinen, A. T.; Sievänen, E.; Laitinen, R. Dissolution behavior of co-amorphous amino acid-indomethacin mixtures: The ability of amino acids to stabilize the supersaturated state of indomethacin. *Eur. J. Pharm. Biopharm.* **2017**, *112*, 85−95.
(40) Koh, Y. P.; Gao, S. Y.; Simon, S. L. Structural recovery of a single polystyrene thin film using Flash DSC at low aging temperatures. *Polymer* **2016**, *96*, 182−187.
(41) Zhou, D. L.; Zhang, G. G. Z.; Law, D.; Grant, D. J. W.; Schmitt, E. A. Physical stability of amorphous pharmaceuticals: Importance of configurational thermodynamic quantities and molecular mobility. *J. Pharm. Sci.* **2002**, *91*, 1863−1872.
(42) Hancock, B. C.; Shamblin, S. L.; Zografi, G. Molecular mobility of amorphous pharmaceutical solids below their glass transition temperatures. *Pharm. Res.* **1995**, *12*, 799−806.
(43) Gupta, P.; Thilagavathi, R.; Chakraborti, A. K.; Bansal, A. K. Role of molecular interaction in stability of celecoxib− PVP amorphous systems. *Mol. Pharmaceutics* **2005**, *2*, 384−391.
(44) Taylor, L. S.; Zografi, G. Spectroscopic characterization of interactions between PVP and indomethacin in amorphous molecular dispersions. *Pharm. Res.* **1997**, *14*, 1691−1698.
(45) Kestur, U. S.; Lee, H. Y.; Santiago, D.; Rinaldi, C.; Won, Y.-Y.; Taylor, L. S. Effects of the molecular weight and concentration of polymer additives, and temperature on the melt crystallization kinetics of a small drug molecule. *Cryst. Growth Des.* **2010**, *10*, 3585−3595.
(46) Ishida, H.; Wu, T.; Yu, L. Sudden rise of crystal growth rate of nifedipine near Tg without and with polyvinylpyrrolidone. *J. Pharm. Sci.* **2007**, *96*, 1131−1138.
(47) Yu, L. Amorphous pharmaceutical solids: preparation, characterization and stabilization. *Adv. Drug Delivery Rev.* **2001**, *48*, 27−42.
(48) Cai, T.; Zhu, L.; Yu, L. Crystallization of organic glasses: effects of polymer additives on bulk and surface crystal growth in amorphous nifedipine. *Pharm. Res.* **2011**, *28*, 2458−2466.
(49) Kwei, T. K. The effect of hydrogen bonding on the glass transition temperatures of polymer mixtures. *J. Polym. Sci., Polym. Lett. Ed.* **1984**, *22*, 307−313.
(50) Kalogeras, I. M. Glass Transition Phenomena in Polymer Blends. In *Encyclopedia of Polymer Blends, Volume 3: Structure*; Isayev, A. I., Ed.; Wiley-VCH: Weinheim, Germany, 2016.
(51) Schneider, H. A. Conformational entropy contributions to the glass temperature of blends of miscible polymers. *J. Res. Natl. Inst. Stand. Technol.* **1997**, *102*, 229.
(52) Chu, P. P.; Wu, H.-D. Solid state NMR studies of hydrogen bonding network formation of novolac type phenolic resin and poly (ethylene oxide) blend. *Polymer* **2000**, *41*, 101−109.
(53) Kalogeras, I. M. Description and molecular interpretations of anomalous compositional dependences of the glass transition temperatures in binary organic mixtures. *Thermochim. Acta* **2010**, *509*, 135−146.
(54) Gordon, M.; Taylor, J. S. Ideal copolymers and the second-order transitions of synthetic rubbers. I. Non-crystalline copolymers. *J. Appl. Chem.* **1952**, *2*, 493−500.


https://doi.org/10.1021/acs.molpharmaceut.1c00353
*Mol. Pharmaceutics* XXXX, XXX, XXX−XXX

(55) Gordon, J. M.; Rouse, G. B.; Gibbs, J. H.; Risen, W. M., Jr. The composition dependence of glass transition properties. *J. Chem. Phys.* **1977**, *66*, 4971−4976.
(56) Kelley, F. N.; Bueche, F. Viscosity and glass temperature relations for polymer-diluent systems. *J. Polym. Sci.* **1961**, *50*, 549−556.
(57) Williams, M. L.; Landel, R. F.; Ferry, J. D. The temperature dependence of relaxation mechanisms in amorphous polymers and other glass-forming liquids. *J. Am. Chem. Soc.* **1955**, *77*, 3701−3707.
(58) Gibbs, J. H.; DiMarzio, E. A. Nature of the glass transition and the glassy state. *J. Chem. Phys.* **1958**, *28*, 373−383.
(59) Pinal, R. Entropy of mixing and the glass transition of amorphous mixtures. *Entropy* **2008**, *10*, 207−223.
(60) Couchman, P. R.; Karasz, F. E. A classical thermodynamic discussion of the effect of composition on glass transition temperatures. *Macromolecules* **1978**, *11*, 117−119.
(61) Couchman, P. R. Compositional variation of glass transition temperatures. 2. Application of the thermodynamic theory to compatible polymer blends. *Macromolecules* **1978**, *11*, 1156−1161.
(62) Simha, R.; Boyer, R. F. On a general relation involving the glass temperature and coefficients of expansion of polymers. *J. Chem. Phys.* **1962**, *37*, 1003−1007.
(63) Fox, T. G. Influence of diluent and of copolymer composition on the glass temperature of a poly-mer system. *Bull. Am. Phys. Soc.* **1956**, *1*, 123.
(64) Painter, P. C.; Graf, J. F.; Coleman, M. M. Effect of hydrogen bonding on the enthalpy of mixing and the composition dependence of the glass transition temperature in polymer blends. *Macromolecules* **1991**, *24*, 5630−5638.
(65) Jenckel, E.; Heusch, R. Die erniedrigung der einfriertemperatur organischer gläser durch lösungsmittel. *Kolloid-Z.* **1953**, *130*, 89−105.
(66) Braun, G.; Kovacs, A. J. In *Physics of Non-Crystalline Solids*, Proceedings of the International Conference, Delft; North Holland: Amsterdam, 1964.
(67) Doolittle, A. K. Studies in Newtonian flow. II. The dependence of the viscosity of liquids on free-space. *J. Appl. Phys.* **1951**, *22*, 1471−1475.
(68) Kim, J. H.; Min, B. R.; Kang, Y. S. Thermodynamic model of the glass transition behavior for miscible polymer blends. *Macromolecules* **2006**, *39*, 1297−1299.
(69) Flory, P. J. Thermodynamics of high polymer solutions. *J. Chem. Phys.* **1942**, *10*, 51−61.
(70) Huggins, M. L. Some properties of solutions of long-chain compounds. *J. Phys. Chem. A* **1942**, *46*, 151−158.
(71) Oishi, T.; Prausnitz, J. M. Estimation of solvent activities in polymer solutions using a group-contribution method. *Ind. Eng. Chem. Process Des. Dev.* **1978**, *17*, 333−339.
(72) Chen, C.-C. A segment-based local composition model for the Gibbs energy of polymer solutions. *Fluid Phase Equilib.* **1993**, *83*, 301−312.
(73) Fu, Y.-H.; Sandler, S. I.; Orbey, H. A modified UNIQUAC model that includes hydrogen bonding. *Ind. Eng. Chem. Res.* **1995**, *34*, 4351−4363.
(74) Hilal, S. H.; Karickhoff, S. W.; Carreira, L. A. Prediction of the solubility, activity coefficient and liquid/liquid partition coefficient of organic compounds. *QSAR Comb. Sci.* **2004**, *23*, 709−720.
(75) Bharti, A.; Banerjee, T. Enhancement of bio-oil derived chemicals in aqueous phase using ionic liquids: Experimental and COSMO-SAC predictions using a modified hydrogen bonding expression. *Fluid Phase Equilib.* **2015**, *400*, 27−37.
(76) Frank, T. C.; Anderson, J. J.; Olson, J. D.; Eckert, C. A. Application of MOSCED and UNIFAC to screen hydrophobic solvents for extraction of hydrogen-bonding organics from aqueous solution. *Ind. Eng. Chem. Res.* **2007**, *46*, 4621−4625.
(77) Chen, C.-C.; Song, Y. H. Generalized electrolyte-NRTL model for mixed-solvent electrolyte systems. *AIChE J.* **2004**, *50*, 1928−1941.
(78) Lewis, G. N.; Randall, M. The activity coefficient of strong electrolytes. *J. Am. Chem. Soc.* **1921**, *43*, 1112−1154.
(79) Lin, Y.; Kate, A.; Mooijer, M.; Delgado, J.; Fosbøl, P. L.; Thomsen, K. Comparison of activity coefficient models for electrolyte systems. *AIChE J.* **2010**, *56*, 1334−1351.
(80) Raatikainen, T.; Laaksonen, A. Application of several activity coefficient models to water-organic-electrolyte aerosols of atmospheric interest. *Atmos. Chem. Phys.* **2005**, *5*, 2475−2495.
(81) Tan, S. P.; Adidharma, H.; Radosz, M. Generalized procedure for estimating the fractions of nonbonded associating molecules and their derivatives in thermodynamic perturbation theory. *Ind. Eng. Chem. Res.* **2004**, *43*, 203−208.
(82) Hao, Y. F.; Chen, C.-C. Nonrandom two-liquid activity coefficient model with association theory. *AIChE J.* **2021**, *67*, No. e17061.
(83) Domańska, U. Experimental data of fluid phase equilibria-correlation and prediction models: a review. *Processes* **2019**, *7*, No. 277.
(84) Mirheydari, S. N.; Barzegar-Jalali, M.; Acree, W. E.; Shekaari, H.; Shayanfar, A.; Jouyban, A. Comparison of the models for correlation of drug solubility in ethanol + water binary mixtures. *J. Solution Chem.* **2019**, *48*, 1079−1104.
(85) Margules, M. Uber die zusammensetzung der gesattigten dampfe von mischungen. *Sitzungsber. Akad. Wiss. Wien, Math.-Naturwiss. Kl.* **1895**, *104*, 1243−1278.
(86) Redlich, O.; Kister, A. T. Algebraic representation of thermodynamic properties and the classification of solutions. *Ind. Eng. Chem.* **1948**, *40*, 345−348.
(87) Renon, H.; Prausnitz, J. M. Local compositions in thermodynamic excess functions for liquid mixtures. *AIChE J.* **1968**, *14*, 135−144.
(88) Wilson, G. M. Vapor-liquid equilibrium. XI. A new expression for the excess free energy of mixing. *J. Am. Chem. Soc.* **1964**, *86*, 127−130.
(89) Zhang, Z.-g.; Huang, D.-h.; Lv, M.; Jia, P.; Sun, D.-z.; Li, W.-x. Entrainer selection for separating tetrahydrofuran/water azeotropic mixture by extractive distillation. *Sep. Purif. Technol.* **2014**, *122*, 73−77.
(90) Kamgar, A.; Esmaeilzadeh, F. Prediction of H2S solubility in [hmim][Pf6],[hmim][Bf4] and [hmim][Tf2N] using UNIQUAC, NRTL and COSMO-RS. *J. Mol. Liq.* **2016**, *220*, 631−634.
(91) Lee, M.-J.; Tsai, L.-H.; Hong, G.-B.; Lin, H.-M. Multiphase equilibria for binary and ternary mixtures containing propionic acid, n-butanol, butyl propionate, and water. *Fluid Phase Equilib.* **2004**, *216*, 219−228.
(92) Müller, E. A.; Gubbins, K. E. Molecular-based equations of state for associating fluids: A review of SAFT and related approaches. *Ind. Eng. Chem. Res.* **2001**, *40*, 2193−2211.
(93) Ferreira, O.; Macedo, E. A.; Bottini, S. B. Extension of the A-UNIFAC model to mixtures of cross-and self-associating compounds. *Fluid Phase Equilib.* **2005**, *227*, 165−176.
(94) Chapman, W. G.; Gubbins, K. E.; Jackson, G.; Radosz, M. New reference equation of state for associating liquids. *Ind. Eng. Chem. Res.* **1990**, *29*, 1709−1721.
(95) Wertheim, M. S. Fluids with highly directional attractive forces. II. Thermodynamic perturbation theory and integral equations. *J. Stat. Phys.* **1984**, *35*, 35−47.
(96) Wertheim, M. S. Fluids with highly directional attractive forces. IV. Equilibrium polymerization. *J. Stat. Phys.* **1986**, *42*, 477−492.
(97) Bondi, A. A. *Physical Properties of Molecular Crystals Liquids, and Glasses*; Wiley: New York, 1968.
(98) National Center for Biotechnology Information. PubChem Compound Summary for CID 3715, Indomethacin, PubChem. https://pubchem.ncbi.nlm.nih.gov/compound/Indomethacin#section=Computed-Properties&fullscreen=true (accessed Feb 22, 2021).
(99) National Center for Biotechnology Information. PubChem Compound Summary for CID 3488, Glyburide, PubChem. https://pubchem.ncbi.nlm.nih.gov/compound/Glyburide#section=Computed-Properties&fullscreen=true (accessed Feb 22, 2021).


https://doi.org/10.1021/acs.molpharmaceut.1c00353
*Mol. Pharmaceutics* XXXX, XXX, XXX−XXX

(100) National Center for Biotechnology Information. PubChem Compound Summary for CID 6322, Arginine, PubChem. https://pubchem.ncbi.nlm.nih.gov/compound/Arginine#section=Computed-Properties&fullscreen=true (accessed Feb 22, 2021).
(101) National Center for Biotechnology Information. PubChem Compound Summary for CID 1983, Acetaminophen, PubChem. https://pubchem.ncbi.nlm.nih.gov/compound/Acetaminophen#section=Computed-Properties&fullscreen=true (accessed Feb 22, 2021).
(102) National Center for Biotechnology Information. PubChem Compound Summary for CID 5288209, Fenretinide, PubChem. https://pubchem.ncbi.nlm.nih.gov/compound/Fenretinide#section=Computed-Properties&fullscreen=true (accessed Feb 22, 2021).
(103) National Center for Biotechnology Information. PubChem Compound Summary for CID 221493, Cholic Acid, PubChem. https://pubchem.ncbi.nlm.nih.gov/compound/Cholic-acid#section=Computed-Properties&fullscreen=true (accessed Feb 22, 2021).
(104) Curry, H. B. The method of steepest descent for non-linear minimization problems. *Q. Appl. Math.* **1944**, *2*, 258−261.
(105) Pajula, K.; Wittoek, L.; Lehto, V. P.; Ketolainen, J.; Korhonen, O. Phase separation in coamorphous systems: in silico prediction and the experimental challenge of detection. *Mol. Pharmaceutics* **2014**, *11*, 2271−2279.
(106) Tool, A. Q. Relation between inelastic deformability and thermal expansion of glass in its annealing range. *J. Am. Ceram. Soc.* **1946**, *29*, 240−253.
(107) Moynihan, C. T.; Easteal, A. J.; De Bolt, M. A.; Tucker, J. Dependence of the fictive temperature of glass on cooling rate. *J. Am. Ceram. Soc.* **1976**, *59*, 12−16.
(108) Badrinarayanan, P.; Zheng, W.; Li, Q. X.; Simon, S. L. The glass transition temperature versus the fictive temperature. *J. Non-Cryst. Solids* **2007**, *353*, 2603−2612.
(109) Plazek, D. J.; Frund, Z. N., Jr. Epoxy resins (DGEBA): The curing and physical aging process. *J. Polym. Sci., Part B: Polym. Phys.* **1990**, *28*, 431−448.
(110) Domańska, U.; Pobudkowska, A.; Pelczarska, A.; Gierycz, P. pKa and solubility of drugs in water, ethanol, and 1-octanol. *J. Phys. Chem. B* **2009**, *113*, 8941−8947.
(111) Bowden, N. A.; Sevillano, D. M.; Sanders, J. P. M.; Bruins, M. E. Modelling the effects of ethanol on the solubility of the proteinogenic amino acids with the NRTL, Gude and Jouyban-Acree models. *Fluid Phase Equilib.* **2018**, *459*, 158−169.
(112) Löbmann, K.; Strachan, C.; Grohganz, H.; Rades, T.; Korhonen, O.; Laitinen, R. Co-amorphous simvastatin and glipizide combinations show improved physical stability without evidence of intermolecular interactions. *Eur. J. Pharm. Biopharm.* **2012**, *81*, 159−169.
(113) Abu-Diak, O. A.; Jones, D. S.; Andrews, G. P. Understanding the performance of melt-extruded poly (ethylene oxide)−bicalutamide solid dispersions: characterisation of microstructural properties using thermal, spectroscopic and drug release methods. *J. Pharm. Sci.* **2012**, *101*, 200−213.
(114) Ravichandran, A.; Khare, R.; Chen, C.-C. Predicting NRTL binary interaction parameters from molecular simulations. *AIChE J.* **2018**, *64*, 2758−2769.
(115) Ravichandran, A.; Tun, H.; Khare, R.; Chen, C.-C. Prediction of thermodynamic properties of organic mixtures: Combining molecular simulations with classical thermodynamics. *Fluid Phase Equilib.* **2020**, *523*, No. 112759.
(116) Fredenslund, A.; Jones, R. L.; Prausnitz, J. M. Group-contribution estimation of activity coefficients in nonideal liquid mixtures. *AIChE J.* **1975**, *21*, 1086−1099.
(117) Chen, C.-C.; Crafts, P. A. Correlation and prediction of drug molecule solubility in mixed solvent systems with the nonrandom two-liquid segment activity coefficient (NRTL− SAC) model. *Ind. Eng. Chem. Res.* **2006**, *45*, 4816−4824.
(118) Chen, C.-C.; Song, Y. H. Solubility modeling with a nonrandom two-liquid segment activity coefficient model. *Ind. Eng. Chem. Res.* **2004**, *43*, 8354−8362.
(119) Hao, Y. F.; Chen, C.-C. Nonrandom Two-Liquid Segment Activity Coefficient Model with Association Theory. *Ind. Eng. Chem. Res.* **2019**, *58*, 12773−12786.
(120) Valavi, M.; Svärd, M.; Rasmuson, Å. C. Prediction of the solubility of medium-sized pharmaceutical compounds using a temperature-dependent NRTL-SAC model. *Ind. Eng. Chem. Res.* **2016**, *55*, 11150−11159.
(121) Tung, H.-H.; Tabora, J.; Variankaval, N.; Bakken, D.; Chen, C.-C. Prediction of pharmaceutical solubility via NRTL-SAC and COSMO-SAC. *J. Pharm. Sci.* **2008**, *97*, 1813−1820.
(122) Sheikholeslamzadeh, E.; Rohani, S. Solubility prediction of pharmaceutical and chemical compounds in pure and mixed solvents using predictive models. *Ind. Eng. Chem. Res.* **2012**, *51*, 464−473.


https://doi.org/10.1021/acs.molpharmaceut.1c00353
*Mol. Pharmaceutics* XXXX, XXX, XXX−XXX